Volume 36, 2013

Papers in Applied Geography

Editors:

Jay Lee
Dawna L. Cerney

REMOTE SENSING OF EVAPOTRANSPIRATION IN FLORIDA USING DRY PIXEL CALIBRATION

Aaron Evans (aevans26@my.fau.edu)
Department of Geosciences, Florida Atlantic University
Boca Raton, FL 33431. Email: aevans26@fau.edu

1. INTRODUCTION

Remote sensing can be a valuable tool for mapping the spatial variability of evapotranspiration (ET) in heterogeneous environments. ET can vary quite abruptly in space due to changes in the availability of water, roughness of the surface, and availability of energy. Eddy covariance towers measure evapotranspiration over a small footprint usually less than 1 km^2 (Kormann and Meixner, 2001). Using them in interpolation is impossible because they are too sparse. Remote sensing cannot directly measure the atmospheric boundary layer because it is too thin. Fortunately, remotely sensed surface information can be used in conjunction with atmospheric forcing measured via surface weather stations to estimate ET flux (Laymon and Quattrochi, 2004).

Different methods have been developed for measuring ET using remote sensing. Typically these methods are physically based although at least one empirically based technique has been developed consisting of training support vector machine with eddy flux data (Yang, 2006). The physical methods can be divided into direct methods (Fisher *et al*., 2008; Mu, 2011) and the residual method. Direct methods attempt to directly calculate ET while the residual method finds ET by subtracting sensible heat (H) from available energy (A). The residual method is an energy balance approach which takes advantage of evaporative cooling in order to partition the available energy between latent and sensible heats flux. ALEXI-DISALEXI (Anderson, 1997) is based on this but incorporates a two-source model which divides ET between evaporation from the soil and transpiration from vegetation. As with direct methods, it requires complex modeling of atmospheric boundary layer and surface/vegetation along with estimation of several model parameters. Although one-source models may not represent physics of ET as precisely, their simplicity can be advantageous when calibrated using in-situ data such as with SEBAL-METRIC (Bastiaanssen, 1998; Allen, 2011). Calibration mitigates inaccuracies in surface temperature retrievals due to atmospheric and emissivity effects. It can also reduce errors introduced by using radiant temperature when aerodynamic temperature is required in the model. Lastly, calibration data provides information about the boundary layer temperature which is required for determining sensible heat (H) in the atmosphere. The equation used in the residual method is of the form:

$$ET = A - H = A - g_a \Delta T = A - g_a (T_{aero} - T_a) \quad [1]$$

where ET is evapotranspiration, A is total available energy from radiation, H is the sensible heat, g_a is the conductivity of the atmosphere, ΔT is the vertical temperature gradient, T_{aero} is the near surface aerodynamic temperature and T_a is the temperature at reference height in boundary layer. Available energy can be estimated using long-wave and shortwave radiance detected by satellite sensor while g_a can be inferred from surface characteristics. Because of difficulties in estimating T_{aero} and T_a, a relationship between ΔT and retrieved surface temperature (T_s) is assumed (Bastiaanssen, 1998):

$$\Delta T = a + b\, T_s \quad [2]$$

Calibration of equation 2 consists of finding dry pixels and wet pixels on an image in which $\Delta T=H/g_a$ information can be estimated. This information is then used to fit the parameters a and b. Determining dry pixel information is typically determined by using expert knowledge to look for dry areas on the image and then assuming that H=A in these spots. Determining dry pixels in this manner can be rather difficult and depends on the skill of the analyst. An automated algorithm for determining dry pixels is highly desirable.

Eddy covariance towers make a good source of data for wet pixel information but it has limited availability. This means the extent of maps calibrated from them are limited to local areas near the stations. Also, it is difficult to split the limited data between calibration and validation when only two or three locations exist in one area. Therefore, it is also highly desirable to develop an algorithm in which **only** dry pixels are used in the calibration allowing eddy covariance data to be used to validate a technique before extending it to areas without tower data.

In this paper an algorithm is proposed for calibrating equation 2 using **only** dry pixels. This approach takes advantage of the relationship between albedo (α) and temperature (T_s) for dry pixels. S-SEBI (Roernik *et al*., 2000) uses the relationship between T_s and α to account for the sensitivity of evaporative fraction of available energy (EF) to available energy itself, but it still requires wet pixel information. The method proposed here allows visualization of dry pixels by plotting available energy (or A/g_a) against T_s. The plot reveals a warm boundary with a sideways "V" pattern where the lower edge of the "V" is made up of dry pixels (skip ahead to Figure 2 for an example). The points forming this lower edge can be found using automated techniques and used to fit parameters a and b in equation 2. Estimations of ET using equations 1 and 2 can now be compared to eddy covariance data for validation.

2. STUDY AREA AND DATA

The proposed calibration method will be tested on a study area outside of Gainesville, FL near Waldo, FL. In this study area two eddy covariance towers are operating with data distributed via the Ameriflux network at http://ameriflux.ornl.gov/. Eddy covariance data consists of 15-minute averaged net radiation, ground flux, friction velocity, sensible heat flux and latent heat flux. Both towers are located over slash pine plantations in various stages of regeneration. Donaldson had a stand age of 25 years in 2012 with canopy height of 14 m in 2008. Mize had a stand age of 13 years in 2012 with canopy height of 10 m in 2008. Donaldson tower height is 24.3 m and Mize tower height is 18.5 m which results in an average fetch on the order of 1 km for both. LANDSAT TM-5 imagery captured on April 23, 2008 at 15:30 GMT consisting of visible, Near IR, SW IR and thermal IR bands was downloaded from http://earthexplorer.usgs.gov/. The thermal band is 120 m resolution and all other bands are 30 m resolution. Figure 1 shows a gray-scale image of visible bands along with the flux tower locations.

3. METHODS

The method in which the proposed calibration algorithm is applied in this study is SEBAL-METRIC. In a nutshell this method requires surface temperature (T_s), available energy (A) and atmospheric conductance (g_a) for use in equations 1 and 2. (Kosa, 2011) contains details on computation of T_s, A and g_a using LANDSAT. Reflective radiance is used to calculate incoming SW radiation and albedo while thermal radiance is used to retrieve T_s. Although surface emissivity (ε) does vary in space, it assumed that $\varepsilon = 0.97$. Often ε is calculated empirically using NDVI but this can produce erratic results without local calibration. Down-welling LW radiation is estimated using cold pixel from image. The fraction of net radiation going to ground heat flux is calculated using SEBAL (Bastiaanssen, 2000). It is understood that there will be uncertainties in calculating the available energy (A) but hopefully it will be consistent in a relative sense. In order to find the conductance of the atmosphere (g_a) similarity theory is applied according to SEBAL-METRIC. The roughness length with respect

to heat is not needed since SEBAL defines temperature gradient between 0.1 m and 2 m. The roughness length with respect to momentum (z_o) is required for determining g_a.

If it is assumed that the roughness of the surface is constant then the following equation can be used for dry pixel calibration:

$$H = a + b\ T_s \quad [3]$$

In order to apply our dry pixel only calibration, available energy is plotted against temperature to reveal the sideways V pattern described earlier. Points in the warm boundary are found by dividing points into bins based on available energy. The maximum T_s in each bin forms the warm boundary. The boundary consists of a decreasing top line and an increasing bottom line that intersect at a threshold energy value. Points with available energy above the threshold are assigned to the top line and all others are assigned to the bottom line. This division is used to fit two straight lines using ordinary least squares regression. The sum of squared errors of the two fits is combined and used as optimization criteria for finding the optimal available energy threshold value. The bottom line is the fit for equation 3 and hereafter called the "dry line". It should also be noted that a simple soil-water balance model (Tasumi, 2003) using precipitation and soil data was used over select "hot spots" as shown in Figure 1 to insure that bare soil should actually be dry. Well data also showed that the water table was not high enough to supply soil evaporation. As shown in Figure 1, dry spots were visually selected in order to compare visual selection to the automated selection.

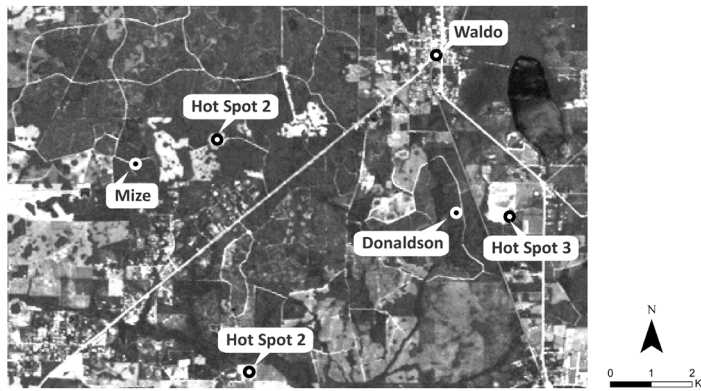

FIGURE 1
STUDY AREA NEAR WALDO, FL ON APRIL 23, 2008
WITH EDDY FLUX TOWER AND VISUALLY CHOSEN HOTSPOTS

In areas with significant changes in obstacle heights, roughness length (z_o) cannot be assumed to be constant. In this case equation 2 must be used and z_o must be estimated. Determining z_o can be difficult and depends on the frequency and amplitude of the variation of obstacle heights. It has been found that the height of obstacles alone can also be related to z_o (Allen et al, 2011) which makes LIDAR data a possible source of z_o. The strength of this relationship also depends on the variability of heights which for vegetation relate to LAI, FAI, FVC, Stand Density, *etc*. (Tian *et al*., 2011; Schaudt and Dickinson, 2000). In the absence of LIDAR data, a relationship between z_o and α can be used (Cho *et al*., 2012):

$$\log(z_o) = -16.8\ \alpha + 1.87 \quad [4]$$

This equation works because taller vegetation typically absorbs more light than shorter vegetation. It was developed empirically using eddy covariance data from around the world. A local calibration of the relationship would be preferred but local z_o for calibration is not

available. It should also be noted that this relationship applies to vegetation and not built up areas where roughness and albedo are not necessarily correlated. This will lead to errors over man-made surfaces. Because water has a low albedo but is smooth, it was masked out of image using minimum distance supervised classification and assigned z_o=0.0001 m. Also, it is assumed that non-water pixels have a minimum z_o=.001 m.

In order to fit equation 2, $\Delta T_{dry}=A/g_a$ is calculated and plotted against T_s. ΔT_{dry} is equal to the temperature gradient that would be observed if the surface was dry. The cases that are actually dry will form the warm lower boundary. The same algorithm described above to fit equation 3 is now used on this data. It is important to note that it is necessary to mask out water during this calibration because it has very high energy and very low conductance which produce clusters of points far above the desired sideways V of data which significantly affects the fit. In addition, the relationship in equation 4 cannot really be trusted over bare/dry areas (especially those recently cleared and littered with debris). Therefore a variation is proposed in which roughness used for calibration is set to constant z_o = 0.001. Of course this z_o is only used in the g_a used to find ΔT_{dry}. The g_a used in equation 1 to produce final ET map must use z_o from equation 4. The idea is that true bare/dry areas will have z_o = 0.001 and lie on the "dry line" as they should. Rougher areas will now have g_a lower than actual which pulls their ΔT_{dry} above the "dry line". Wet regions will also be pulled further above "dry line" but dry/rough areas that should be on the "dry line" will also be taken away. As long as there is enough smooth/dry pixels this will be good since it eliminates the rough/dry pixels which can't be trusted. One thing to notice here is that a minority of pixels is used to fit this "dry line" and measures must be taken to keep corrupt pixels out. Later, these corrupt pixels might produce anomalous ET values in the final map, but if they are a minority they will not affect ET at the image level.

Eddy covariance data is used to validate the 3 calibration variations which will be denoted as 1) H calibration 2) ΔT calibration and 3) ΔT fixed z_o calibration. Eddy covariance data is notorious for underestimating fluxes because it fails to capture low frequency turbulence (Foken, 2008). This paper adopts the current working solution of assuming that H and ET are reduced similarly so that the Evaporative Fraction (EF) = ET/(H+ET) is close to actual. Also, eddy flux towers measure a weighted average of an upwind source over a footprint resembling a bellshape (Kormann and Meixner, 2001). Since the area around Mize and Donaldson towers is not too variable, a uniform 1 km footprint is used. It turns out that the flux footprint is inconsistent with the available energy (A_{TOWER}) footprint. In addition, A_{TOWER} will contain different sources of error compared to $A_{LANDSAT}$ and therefore $A_{LANDSAT}$ will be used to maintain consistency. In effect what is being compared now is EF. In order to find predicted footprint EF to compare to EF_{TOWER}, parameters must be averaged over footprint:

$$EF_{PREDICTED} = 1 - \frac{a\,\overline{g_a} + b\,\overline{T_s\,g_a}}{\overline{A}} \qquad [5]$$

where the over bar represents the average over the footprint. Since a and b were fit based on available energy (A), some of the inaccuracies of A will now be in the top and bottom of the second term in equation 5 and could cancel out making EF more reliable. EF is also useful measure because it has been determined to be relatively constant throughout the day (Llhome, 1999). Therefore, a snapshot of EF can be multiplied by the daily averaged source of available energy such as GOES (Mecikalski *et al*., 2011) to get daily ET. Producing maps of EF is as easy as applying equation 1 and equation 2 or 3 to maps of T_s, A and g_a.

4. RESULTS AND DISCUSSION

Figure 2 shows the plot of A vs T_s created for the H calibration of equation 3. There is a fairly clear warm boundary producing the sideways V pattern. In the dry areas, as the surface becomes darker and the available energy increases, the temperature also increases. But, once the surface becomes vegetated, the temperature actually decreases as available energy increases which might seem counter intuitive. This is occurring because the cooling effect due to the increase in transpiration is greater than the warming due to low albedo of vegetation. The

bottom "dry line" represents sensible heat as a function of temperature. The validation points of sensible heat at the towers plotted on Figure 2 are far above the "dry line" demonstrating considerable error in this variation. The reason for this is because this model neglects variations in surface roughness. The slope of the dry line is equal to the conductance of atmosphere which increases with roughness (see equation 1). Therefore, since the towers are measured over slash pines which are very rough, the relationship between H and T should have a greater slope as shown by straight lines passing through tower points. Also the point in Waldo is over a one story building which should have a greater slope (rougher) than the "dry line" presumably over bare ground. It is also interesting to note that the visually detected hot spots also appear rougher than "dry line". All of this demonstrates the importance of including the surface roughness in the algorithm.

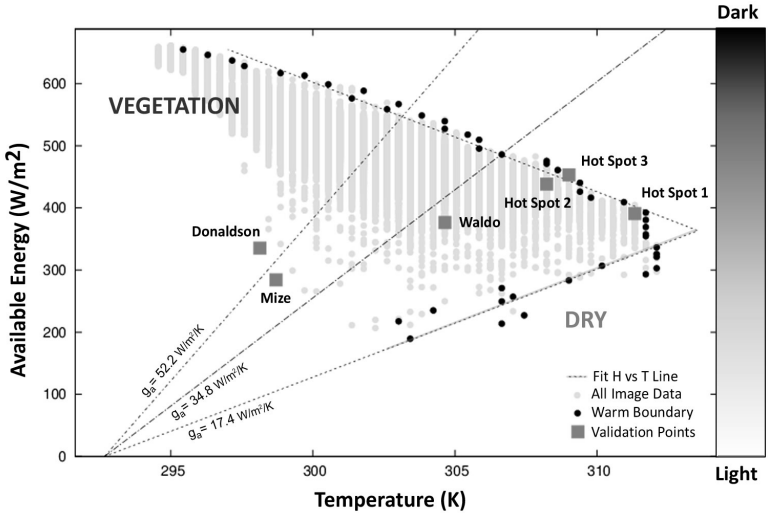

FIGURE 2
VISUALIZATION OF H CALIBRATION VARIATION

Figure 3 shows the plot of ΔT_{dry} vs T_s for the ΔT calibration of equation 2. Now the validation points better match the predicted "dry line" because surface roughness is accounted for. It is also obvious that Waldo is a bad fit because the roughness assigned to it using equation 4 works poorly over manmade surfaces. Also, some of the visually detected hot spots are off probably due to failures with equation 4 over these cleared areas. Figure 4 shows the results for the ΔT fixed z_o calibration. In this variation the eddy covariance validation ΔT points line up even better with the predicted dry line. Waldo and Hot Spot 2 are still off probably due to roughness. Also, Google images show some level of re-growth at Hot Spot 2 that is hard to detect from LANDSAT. Therefore non-zero ET should be used for that point which would bring ΔT down from what is plotted. This shows that visually selecting dry spots from imagery is not the best way to find them. It is beneficial that the z_o calibration variation works well because it does not rely on accurate z_o. When z_o is calculated from equation 4 there can be large discrepancies over bare/dry areas introducing errors to the minority of points used for calibration. By fixing z_o=0.001, rougher points will be removed from calibration data and this is a good thing as long as relatively smooth areas exist. It is true that there will be errors due to roughness length in the final ET map but this will be ok if they make up a small area of the map. But on the contrary, introducing even a small number of them to the calibration could alter the entire ET map as demonstrated in Figure 3 which has a bias toward Donaldson. In addition, areas that are considered dry based on a value such as NDVI could be assigned ET = 0 when producing final ET map.

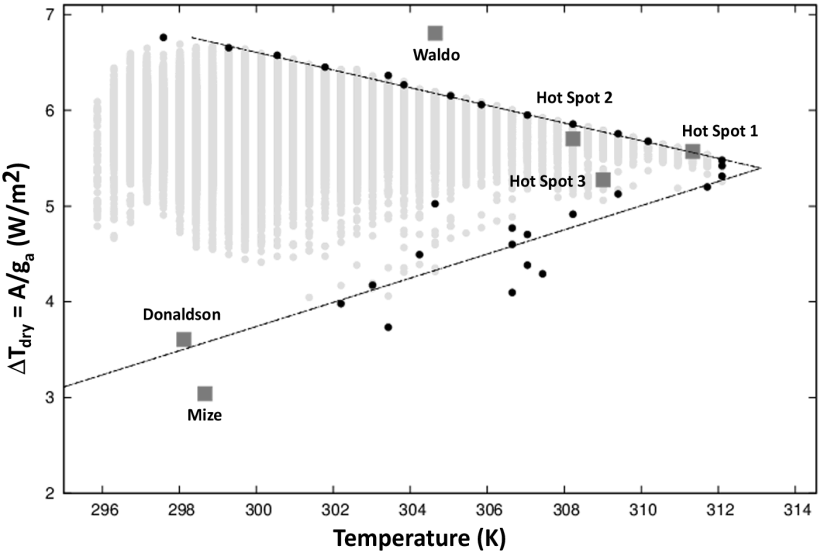

FIGURE 3
VISUALIZATION OF ΔT CALIBRATION VARIATION

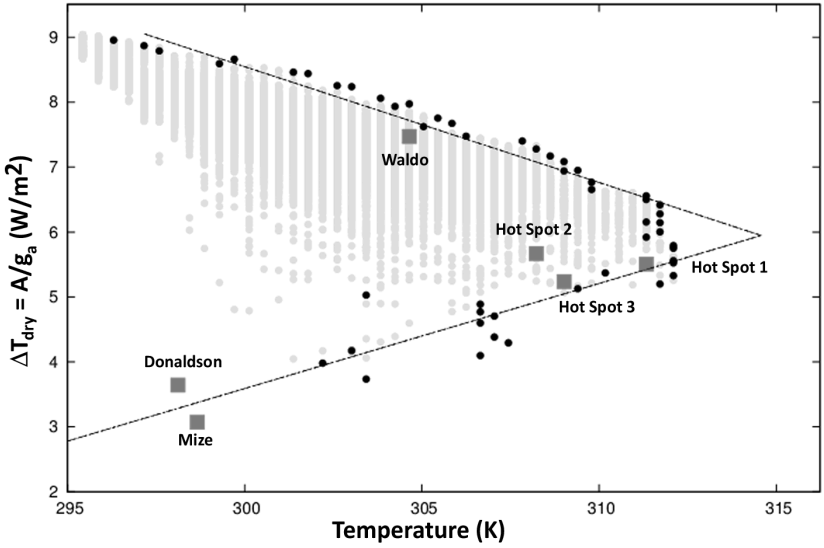

FIGURE 4
VISUALIZATION OF ΔT FIXED Z_O CALIBRATION VARIATION

The values used for validation ET (in latent heat units) are 237.0 W/m^2 at Donaldson and 281.9 W/m^2 at Mize. The evaporative fraction (EF) from eddy covariance data for Donaldson equals 41.4% and Mize equals 49.8%. Table 1 shows the bias and mean absolute errors between the validation ET and the remotely sensed ET after integrating over footprint using equation 5. The validation ET is calculated by multiplying eddy covariance ET by remotely sensed available energy. Therefore, the errors in Table 1 do not reflect inaccuracies in

remotely sensing available energy but instead represent the algorithms ability to detect EF. The results are displayed as ET in order to represent the effect that errors in EF have on ET.

TABLE 1
BIAS AND MAE FOR CALIBRATION VARIATIONS

Variation	BIAS	MAE
H Calibration	209.4 (80.7 %)	209.4 (80.7 %)
ΔT Calibration	-20.2 (-7.8 %)	29.5 (11.3 %)
ΔT Fixed Z_o	2.6 (1.0 %)	30.5 (11.8 %)

The H calibration variation is clearly ineffective demonstrating the importance of including roughness length in the algorithm. The retrieved ET is almost double the observed values. Both ΔT calibrations produce much better results. The ΔT fixed z_o calibration seems too good to be true. Such a nearly perfect agreement is probably a bit of luck and warrants application of the algorithm to additional dates and locations. It is also important to remember that some of the errors associated with the eddy covariance method did not cancel out as well as planned. It is good news that the ΔT fixed z_o calibration worked as well as the original ΔT calibration because it should be less affected by problems associated with finding z_o.

Figure 5 is the map of evaporative fraction produced using the ΔT fixed z_o calibration. Mapping EF gives a sense of the availability of water in the landscape. The algorithm was able to distinguish areas of runoff from areas of slash pine. The built up areas are not represented well because of the under estimation of roughness as discussed before. After looking at a false color composite, some of the other cleared out areas seem to have larger than expected EF. Possibly these areas are truly more vegetated/wet than it seems or maybe they are just rougher than predicted. Additional ground truthing would be of great value here. The dry pixels that the algorithm selected for calibration are also shown on Figure 5. Most of the points chosen are on the southwest corner of the map. The limited spatial coverage of calibration points could reveal a potential weakness in the dry pixel calibration. In different landscapes will suitable calibration points also be available?

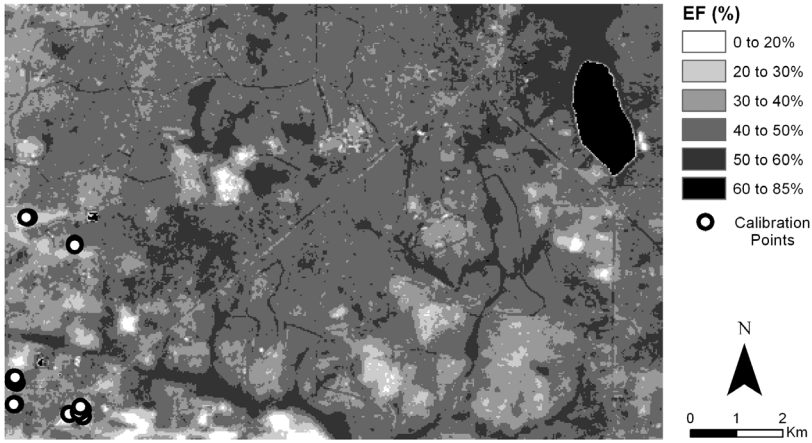

FIGURE 5
EF MAP USING ΔT FIXED Z_O CALIBRATION VARIATION

Field scale maps such as Figure 5 could be used by managers to determine water use or productivity of ecosystems. In this particular instance the effect of logging on the hydrologic balance could be monitored. By looking at a time series of images the change in

water lost from the landscape could be quantified. By automating the calibration, the resources required for processing these time series is significantly reduced. This allows the estimation of monthly ET to become operational. These monthly ET products can be input into ground and surface water models in order to quantify effects of land use change. Another important application of Figure 5 is mapping the fraction of reference ET (EF_{RET}). Reference ET (RET) is the ET over a well-watered reference crop and is a function of climate only (Allen, *et al*., 2011). Managers can make projections of climate change and multiply corresponding RET by maps of EF_{RET} to get future ET. Although Figure 5 is over a small extent and relatively fine resolution, extending these maps to a regional scale would help in planning the management of regional water supplies.

A simple technique for determining EF from a thermal image would be to assume that EF is a linear function of temperature and then calibrate the relationship using wet and dry pixels. (Jiang *et al*., 2009) did this for south Florida by finding a wet and dry temperature using the triangle method. The triangle method consists of plotting NDVI vs. temperature after which the boundaries of the triangle produce the cold (wet) and hot (dry) limits. EF for the dry pixels is assumed to be zero and the wet EF is set equal to potential ET using Priestly-Taylor equation. In a stressed environment it would probably be necessary to find the wet EF using in-situ data. This simple calibration was performed using the eddy covariance data with the visually selected dry pixels to examine the feasibility of this approach. The result is shown in Figure 6. The resulting fit will be very sensitive to the choice of visually inspected hotspots. This line is also compared to the EF calculated using the ΔT fixed z_o calibration technique. The large scatter in EF shows that EF is related to more than just temperature. This could explain why SSEbop (Senay *et al*., 2013), an operational algorithm used by USGS that does not account for roughness, did not validate well with a flux tower at Austin Carey in our study area.

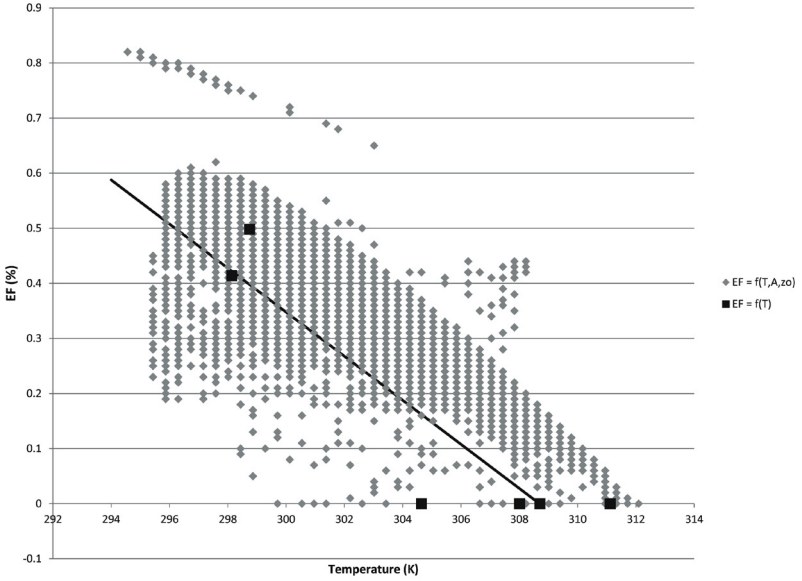

FIGURE 6
EF VS. T USING ΔT FIXED Z_O CALIBRATION
WITH VALIDATION POINTS AND VISUALLY SELECTED HOTSPOTS

5. CONCLUSIONS AND FUTURE WORK

The dry pixel only calibration technique proposed here is worthy of further investigation. Some of the results produced here may be overly optimistic. This is the only

study area where the author has applied this technique. It is important now to apply the technique to additional dates and study areas. This study also demonstrates the importance of accounting for roughness length in terrain with tall canopy. Therefore it is important to produce reliable means of determining roughness length. Another issue to explore is spatial resolution. LANDSAT has a 16 day return period which decreases the number of clear sky days available in a year. MODIS has a daily return period but has a coarser resolution (1 km thermal). For water resource managers interested in computing seasonal ET losses MODIS would offer better temporal resolution. Future work will investigate the applicability of the dry pixel only calibration to MODIS. The problem with this is that MODIS resolution is too coarse to resolve dry only pixels in study areas such as the one investigated in this work. Therefore, a technique must be developed to fuse LANDSAT and MODIS together in a way that dry areas can be resolved.

The SEBAL method uses Monin-Obukhov similarity theory which was derived for homogenous landscapes. More applicable to heterogeneous environments would be to couple large-eddy simulations with remote sensing (Albertson *et al*., 2001). The ALEXI-DISALEXI algorithm cited earlier addresses this by using coarse scale spatial resolution such as GOES (5-10 km) and then "disaggregating" this to finer resolutions LANDSAT or MODIS (Anderson *et al*., 2011). In the future this issue would have to be addressed in the algorithm developed in this study.

The advantage of using a calibration approach is that it reduces some of the modeling and required parameters. The advantage of the dry pixel only calibration as presented here is that it does not require in-situ data which gives it the potential for creating ET maps over a larger extent. This allows available in-situ data to be used for validation. The algorithm also allows for automation of calibration because the end user does not have to pick out hot and cold spots on map. In closing, the results produced in this paper seem to justify further exploration into this type of approach.

6. REFERENCES

Albertson, J. D., Kustas, W.P., and Scanlon, T.M. (2001). Large-eddy simulation over heterogeneous terrain with remotely sensed land surface conditions. *Water Resources Research*, 37(7): 1939–1953.

Allen, R., Irmak, A., Trezza, R. , Hendrickx, J.M.H. , Bastiaanssen, W. and Kjaersgaard, J. (2011). Satellite-based ET estimation in agriculture using SEBAL and METRIC. *Hydrological Processes*. 25: 4011-4027.

Anderson, M. C., Kustas, W. P., Norman, J. M., Hain, C.R., Mecikalski, J. R., Schultz, L., Gonz´alez-Dugo, M. P., Cammalleri, C. , d'Urso, G., Pimstein, A., and Gao, F. (2011). Mapping daily evapotranspiration at field to continental scales using geostationary and polar orbiting satellite imagery. *Hydrology Earth Systems Science*. 15: 223-239.

Anderson, M. C., Norman, J. M., Diak, G. R., Kustas, W. P., and Mecikalski, J. R. (1997). A Two-Source Time Integrated Model for Estimating Surface Fluxes Using Thermal Infrared Remote Sensing. *Remote Sensing of the Environment*, 60: 195-216.

Bastiaanssen, W.G.M., Menentia, M., Feddesb, R.A. and Holtslagc, A.A.M. (1998). A remote sensing surface energy balance algorithm for land (SEBAL) 1. Formulation. *Journal of Hydrology*. 212: 198–212.

Bastiaanssen, W.G.M., Menentia, M., Feddesb, R.A. and Holtslagc, A.A.M. (2000). SEBAL-based sensible and latent heat fluxes in the irrigated Gediz Basin, Turkey. *Journal of Hydrology*. 229: 87–100.

Cho, J., Miyazaki, S., Yeh, J., Kim, W., Kanae, S., and Oki, T. (2012). Testing the hypothesis on the relationship between aerodynamic roughness length and albedo using vegetation structure parameters. *International Journal of Biometeorology*. 56: 411-418.

Fisher, J.B., Tu, K.P., and Baldocchi, D.D. (2008). Global estimates of the land–atmosphere water flux based on monthly AVHRR and ISLSCP-II data, validated at 16 FLUXNET sites. *Remote Sensing of Environment*, 112: 901-919.

Foken, T. (2008). The Energy Balance Closure Problem: An Overview. *Ecological Applications*, 18(6): 1351-1367.

Jiang L., Islam, S., Guo, W., Jutla, A.S., Senarath, S.U.S., Ramsay, B.H., and Eltahir, E. (2009). A satellite-based Daily Actual Evapotranspiration estimation algorithm over South Florida. *Global and Planetary Change*, 67: 62–77.

Kormann, R.and Meixner, F.X. (2001). An Analytical Footprint Model for Non-neutral Stratification. *Boundary-Layer Meteorology*, 99: 207–224.

Kosa, P. (2011) . The Effect of Temperature on Actual Evapotranspiration based on Landsat 5 TM Satellite Imagery (SEBAL). In L. Labedzki (Eds.), *Evapotranspiration* (pp. 209-228). Rijeka, Croatia: InTech.

Layman, C.A., & Quattrochi, D.A. (2004) . Estimating spatially distributed surface fluxes in a semi-arid Great Basin desert using Landsat TM thermal data. In D. Quattrochi & J. Luvall (Eds), *Thermal Remote Sensing in Land Surface Processes* (pp. 133-158). Boca Raton:CRC.

Lhomme, J. P., and Chehbouni, A. (1999). Comments on dual-source vegetation– atmosphere transfer models. *Agricultural and Forest Meteorology*, 94: 269– 273.

Mecikalski, J.R., Sumner, D.M., Jacobs, J.M., Pathak, C.S., Paech, S.J., and Douglas, E.M. (2011) . Use of Visible Geostationary Operational Meteorological Satellite Imagery in Mapping Reference and Potential Evapotranspiration over Florida. In L. Labedzki (Eds.), *Evapotranspiration* (pp. 241-254). Rijeka, Croatia : InTech.

Mu, Q., Zhao,M., and Running,S.W. (2011). Improvements to a MODIS global terrestrial evapotranspiration algorithm. *Remote Sensing of Environment* 115:1781–1800.

Roerink, G., Su, Z., and Menenti, M. (2000). S-SEBI: A Simple Remote Sensing Algorithm to Estimate the Surface Energy Balance. *Physics and Chemistry of the Earth, Oceans and Atmosphere*. 25(2): 147-157.

Schaudt, K.J., and Dickinson, R.E. (2000). An approach to deriving roughness length and zero-plane displacement height from satellite data, prototyped with BOREAS data. *Agricultural and Forest Meteorology* 104: 143–155.

Senay, G.B., Bohms, S., Singh, R.K., Gowda, P.H., Velpuri, N.M., Alemu, H. and Verdin, J.P. (2013) Operational Evapotranspiration Mapping Using Remote Sensing and Weather Datasets: A New Parameterization For the SSEB Approach. *Journal of the American Water Resources Association* 49(3): 577-591.

Tasumi M. 2003. Progress in operational estimation of regional evapotranspiration using satellite imagery. PhD Dissertation, University of Idaho, Moscow, ID; 357.

Tian, X., Li, Z.Y., van der Tol, C., Su, Z. , Li, X., He, Q.S., Bao, Y.F., Chen, E.X., and Li, L.H. (2011).Estimating zero-plane displacement height and aerodynamic roughness length using synthesis of LiDAR and SPOT-5 data. *Remote Sensing of Environment*, 115: 2330–2341.

Yang, F., White, M., Michaelis, A., Ichii, K., Hashimoto, H., Votava, P., Zhu, A. & Nemani, R. (2006). Prediction of Continental-Scale Evapotranspiration by Combining MODIS and AmeriFlux Data Through Support Vector Machine. *IEEE Transactions on Geoscience and Remote Sensing*, 44(11): 3452-3461.